

- After concentration, the protein was passed through an S200 gel filtration column, using running buffer (20 mM Hepes, pH 7.4, 150 mM NaCl, 4 mM DTT). Clathrin and AP2 were purified from fresh pig brain as previously described (34). AP2 was dialyzed against 50 mM triethanolamine-KCl, pH 8.0, 200 mM NaCl, 0.2 mM EDTA, 0.1%  $\beta$ -mercaptoethanol, and 0.02%  $\text{NaN}_3$ . Clathrin cage formation was performed as described previously (6) in 25 mM Hepes, 125 mM K acetate, and 1 mM Mg acetate, pH 7.4.
20. Crystals of CALM-N (residues 1 to 289) were grown in seeded hanging drops against a reservoir containing 0.1 M Hepes, pH 7.5, 12 to 14% PEG 8000, and 8% ethylene glycol. They belong to space group P4<sub>1</sub>2<sub>1</sub>2, cell dimensions  $a = b = 77.93$  Å,  $c = 121.81$  Å, with one molecule per asymmetric unit. For the binding studies, crystals were soaked for 1 hour in 1 mM ligand in 0.1 M Hepes, pH 7.5, 14% PEG 8000, and 8% ethylene glycol. We were unable to find suitable conditions for cryoprotection, so all data sets were collected at room temperature from crystals mounted in capillaries, on beamline 9.6 at SRS Daresbury,  $\lambda = 0.88$  Å. By setting the ADSC Quantum 4 charge-coupled device detector to the fastest readout time (~3 s) and using a 3-s exposure for a 1° rotation, a 90° data set could be collected in less than 10 min with acceptable radiation damage. Images were integrated using Mosflm (35) and scaled using CCP4 programs (36). All data sets extended to 2 Å resolution and were reasonably strong to 2.1 Å resolution (see PDB depositions and Table 1 for details). Phases were derived from a single mercury derivative with two sites (crystals soaked for 1 hour in 1 mM ethylmercury thiosalicylate) by the program Sharp (37). Solvent flattening with Solomon led to an easily interpretable map. The model was built using O (38) and refined using Refmac5 (39). The termini (1 to 19 and 281 to 289) were not visible. Density was weak around the  $\alpha 7$  to  $\alpha 8$  loop (149 to 165); around the  $\alpha 9$  to  $\alpha 10$  loop (215 to 237); and the COOH-terminal region from about 267. Final *R* factors for the native and complexes were 0.187 to 0.195 (*R*<sub>free</sub> 0.215 to 0.230). Coordinates have been deposited in the PDB with access codes 1hf8 (native), 1hfa [PtdIns(4,5)P<sub>2</sub>], 1hg2 [Ins(4,5)P<sub>2</sub>], and 1hg5 (InsP<sub>6</sub>).
21. E. Conti, M. Uy, L. Leighton, G. Blobel, J. Kuriyan, *Cell* **94**, 193 (1998).
22. A. K. Das, P. W. Cohen, D. Barford, *EMBO J.* **17**, 1192 (1998).
23. J. Hyman, H. Chen, P. P. Di Fiore, P. De Camilli, A. T. Brunger, *J. Cell Biol.* **149**, 537 (2000).
24. E. C. Dell'Angelica, J. Klumperman, W. Stoorvogel, J. S. Bonifacino, *Science* **280**, 431 (1998).
25. Single-letter abbreviations for the amino acid residues are as follows: A, Ala; C, Cys; D, Asp; E, Glu; F, Phe; G, Gly; H, His; I, Ile; K, Lys; L, Leu; M, Met; N, Asn; P, Pro; Q, Gln; R, Arg; S, Ser; T, Thr; V, Val; W, Trp; X, any amino acid; and Y, Tyr.
26. T. de Beer, R. E. Carter, K. E. Lobel-Rice, A. Sorkin, M. Overduin, *Science* **281**, 1357 (1998).
27. Lipid tubules [10% PtdIns(4,5)P<sub>2</sub>, 10% cholesterol, 40% phosphatidylcholine, 40% NFA-galactocerebroside type II] were prepared as described in (40). Liposomes [10% PtdIns(4,5)P<sub>2</sub>, 10% PtdSer, 10% cholesterol, 35% phosphatidylcholine, and 35% phosphatidylethanolamine] were prepared by evaporating solvent from an appropriate mixture of lipids under a constant stream of argon. After resuspension in 10 mM Hepes, pH 7.4, the mixtures were extruded through a filter with pore size 0.1  $\mu\text{M}$ . Initially, tubules were used for comparison with our studies on dynamin, whose pleckstrin homology domain binds phosphoinositol head groups (40). Moreover, tubules are easier to sediment than liposomes. Dynamin was also used in the liposome experiments as a positive control for the incorporation of phosphatidyl inositols.
28. Protein(s) and liposomes or tubules (as appropriate) were added to reaction buffer (25 mM Hepes, pH 7.4, 125 mM K acetate, 1 mM Mg acetate) in a polycarbonate centrifuge tube (final volume of each experiment 50 or 100  $\mu\text{l}$ ). Experiments were incubated at room temperature for 30 min before sedimentation by centrifugation (78,000*g* for 20 min in a TLA100 rotor) and analyzed by Coomassie-stained gels. Densitometry was carried out using a Molecular Dynamics scanner and bands were integrated using ImageQuant for Macintosh v1.2.
29. A monolayer of lipid [same composition as 10% PtdIns(4,5)P<sub>2</sub> liposomes] was formed on the surface of a buffer droplet in a Teflon block (41), and the protein(s) of interest were introduced into the buffer. After 5 min, a carbon-coated gold electron microscopy grid was placed onto the monolayer. After 1 hour, the grid was removed and stained with uranyl acetate (2% uranyl acetate, 0.0025% polyacrylic acid). The technique has been used for the generation of two-dimensional crystals (41, 42) and, to our knowledge, has not been applied to study the formation of endocytic intermediates. Potassium in the buffer was critical for the efficient polymerization of clathrin in keeping with previous observations (43).
30. D. J. Owen *et al.*, *Cell* **97**, 805 (1999).
31. L. M. Traub, M. A. Downs, J. L. Westrich, D. H. Fremont, *Proc. Natl. Acad. Sci. U.S.A.* **96**, 8907 (1999).
32. P. Wigge, Y. Vallis, H. T. McMahon, *Curr. Biol.* **7**, 554 (1997).
33. C. E. Futter, A. Pearce, L. J. Hewlett, C. R. Hopkins, *J. Cell Biol.* **132**, 1011 (1996).
34. C. J. Smith, N. Grigorieff, B. M. Pearce, *EMBO J.* **17**, 4943 (1998).
35. A. G. W. Leslie, in *Joint CCP4 and ESF-EACMB Newsletter on Protein Crystallography* No. 26 (SERC, Daresbury Laboratory, Warrington, UK, 1992).
36. Collaborative Computational Project No. 4, *Acta Crystallogr.* **D50**, 760 (1994).
37. E. de la Fortelle, G. Bricogne, *Methods Enzymol.* **276**, 472 (1997).
38. T. A. Jones, J. Y. Zou, S. W. Cowan, M. Kjeldgaard, *Acta Crystallogr.* **A47**, 110 (1991).
39. G. N. Murshudov, A. A. Vagin, E. J. Dodson, *Acta Crystallogr.* **D53**, 240 (1997).
40. M. H. Stowell, B. Marks, P. Wigge, H. T. McMahon, *Nature Cell Biol.* **1**, 27 (1999).
41. D. Levy *et al.*, *J. Struct. Biol.* **127**, 44 (1999).
42. R. D. Kornberg, S. D. Darst, *Curr. Opin. Struct. Biol.* **1**, 642 (1991).
43. J. E. Heuser, R. G. Anderson, *J. Cell Biol.* **108**, 389 (1989).
44. X. Zhao *et al.*, *J. Cell Sci.* **114**, 353 (2001).
45. We thank O. Perisic for advice on liposome preparation, E. Ungewickell for the AP180 clone, L. Serpell and J. Berriman for assistance with platinum shadowing, D. Brodersen and B. Clemons for assistance with data collection, and the staff of beamline 9.6, SRS Daresbury. Also, we thank N. Unwin and members of our labs for extensive discussion.

20 November 2000; accepted 18 December 2000

## Notch Inhibition of RAS Signaling Through MAP Kinase Phosphatase LIP-1 During *C. elegans* Vulval Development

Thomas Berset, Erika Fröhli Hoier, Gopal Battu, Stefano Canevascini, Alex Hajnal\*

During *Caenorhabditis elegans* vulval development, a signal from the anchor cell stimulates the RTK/RAS/MAPK (receptor tyrosine kinase/RAS/mitogen-activated protein kinase) signaling pathway in the closest vulval precursor cell P6.p to induce the primary fate. A lateral signal from P6.p then activates the Notch signaling pathway in the neighboring cells P5.p and P7.p to prevent them from adopting the primary fate and to specify the secondary fate. The MAP kinase phosphatase LIP-1 mediates this lateral inhibition of the primary fate. LIN-12/NOTCH up-regulates *lip-1* transcription in P5.p and P7.p where LIP-1 inactivates the MAP kinase to inhibit primary fate specification. LIP-1 thus links the two signaling pathways to generate a pattern.

MAP kinase phosphatases (MKPs) belong to the family of dual-specificity phosphatases that inactivate different types of MAP kinases by dephosphorylating the critical phosphotyrosine and phosphothreonine residues of the kinases (1). The transcription

of MKPs is rapidly induced by various stimuli such as growth factors and cellular stresses that activate MAP kinases, suggesting that MKPs may participate in an autoinhibitory feedback loop.

To study the role of MKPs in RTK/RAS/MAPK signaling during development, we searched the *C. elegans* genome sequence for homologs of vertebrate MKPs. Among the 185 predicted phosphatases, we identified a candidate, termed *lip-1* (lateral signal induced phosphatase-1, open read-

Division of Cancer Research, Department of Pathology, University of Zürich, Schmelzbergstrasse 12, CH-8091 Zürich, Switzerland.

\*To whom correspondence should be addressed. E-mail: ahajnal@pathol.unizh.ch

## REPORTS

ing frame C05B10.1), that is similar to human MKPs (Fig. 1A). LIP-1 exhibits 32% overall sequence identity and 49% similarity to human MKP-3/PYST1.

Using a polymerase chain reaction (PCR)-based assay to screen a library of ethylmethane sulfonate-mutagenized worms (2), we isolated a deletion in *lip-1* (Fig. 1B). The *zh15* deletion removes 1416 base pairs (bp) that encode the putative MAP kinase binding domain and part of the catalytic domain of LIP-1 including the conserved Asp<sup>236</sup> residue that is required for the proton transfer during the phosphatase reaction (Fig. 1, A and B). Moreover, no *lip-1* transcripts could be detected in *lip-1(zh15)* mutants by Northern blot analysis (Fig. 1C). Thus, the homozygous viable *lip-1(zh15)* mutation probably represents a loss-of-function (*lf*) allele. *lip-1(lf)* animals contained higher levels of MAP kinase enzymatic activity, whereas animals carrying a transgene with a hyperactive form of *lip-1* (*[lip-1::nls::gfp]*, see below) exhibited lower kinase activity when compared with wild type (Fig. 1D). Thus, LIP-1 may negatively regulate MAP kinase activity.

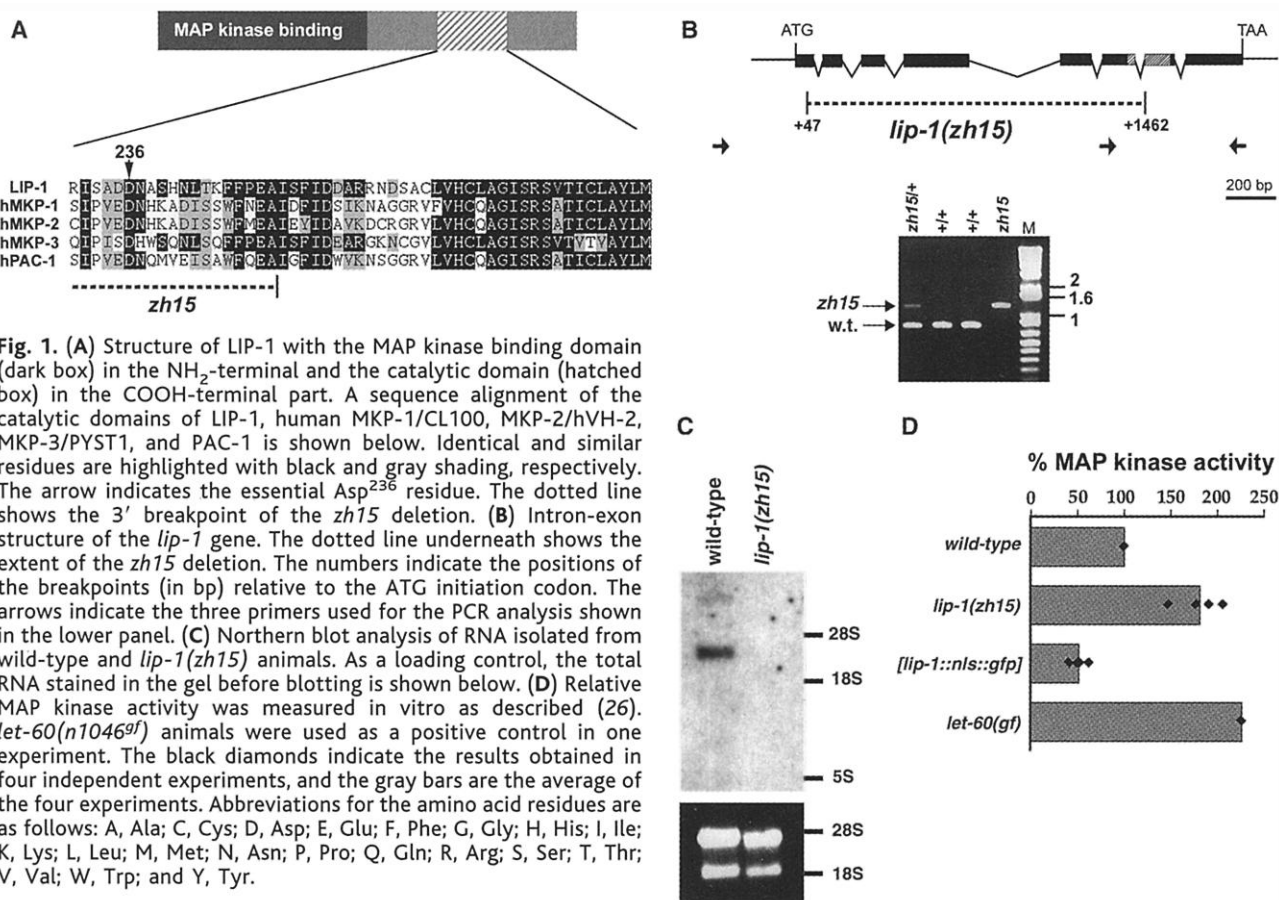
We therefore investigated whether LIP-1 inhibits MAP kinase MPK-1 signaling during vulval induction (3, 4). In *lip-1(lf)* single mutants, vulval development ap-

peared normal (Table 1, row 2). However, loss of *lip-1(+)* function suppressed the vulvaless (Vul) phenotype caused by mutations that partially reduce the activity of the RTK/RAS/MAPK signaling pathway, such as mutations in *let-23 egfr* (5), *lin-7 pdz* (6), *sem-5 grb2* (7), or *mpk-1* MAP kinase (Table 1, rows 3 to 10). Furthermore, animals expressing *mpk-1(+)* under control of the heat-shock promoter (*[HS-mpk-1(+)]*) exhibited wild-type levels of vulval induction at 20°C (8), whereas *lip-1(lf); [HS-mpk-1(+)]* double mutants displayed a strong multivulva (Muv) phenotype (Table 1, rows 11 and 12). Thus, loss of *lip-1(+)* function increases the sensitivity of the vulval precursor cells (VPCs) P3.p through P8.p toward the inductive signal. Consistent with the hypothesis that LIP-1 inhibits MPK-1 signaling, a mutation in *lin-25* that acts downstream of or parallel to *mpk-1* (9) was only weakly suppressed by *lip-1(lf)* (Table 1, rows 13 and 14).

Overexpression of *lip-1(+)* under the control of the Pn.p cell-specific *lin-31* promoter (10) caused a Vul phenotype (Table 1, row 15). Furthermore, whereas animals expressing a *lip-1*-green fluorescent protein (GFP) fusion (*[lip-1::gfp]*) under the control of the *lip-1* promoter only rarely exhibited a Vul phenotype, the insertion of a

nuclear localization signal (*[lip-1::nls::gfp]*) caused a penetrant Vul phenotype (Table 1, rows 16 and 17), suggesting that LIP-1 may act more efficiently when translocated into the nucleus. Using this activated (nuclear) form of LIP-1, we determined at what step LIP-1 inhibits the RTK/RAS/MAPK signaling pathway. The *[lip-1::nls::gfp]* transgene efficiently suppressed the Muv phenotype caused by a *let-60 ras(gf)* mutation (11) or by overexpression of *mpk-1(+)*, but it failed to suppress the *lin-1(rf)* Muv phenotype (Table 1, rows 18 to 23). *lin-1* encodes an ETS-domain transcription factor that inhibits vulval induction downstream of MPK-1 (12). In *lin-1(rf)* mutants, the VPCs adopt vulval fates independently of MPK-1 activity. Thus, LIP-1 inhibits vulval induction upstream of LIN-1, most likely at the level of MPK-1.

To determine the LIP-1 expression pattern, we analyzed two *lip-1::gfp* reporter lines (Fig. 2A). LIP-1::GFP expression was observed in most somatic cells starting during embryogenesis and persisting throughout larval development and adulthood. In particular, LIP-1::GFP was uniformly expressed at a low level in all VPCs until the L2 stage. In early L3 larvae however, LIP-1::GFP expression was up-regulated in the secondary (2°) VPCs P5.p



## REPORTS

and P7.p in 71% of [*lip-1::nls::gfp*] animals (Fig. 2B) ( $n = 24$ ). To examine if the increase in LIP-1 expression was regulated at the level of transcription, we inserted a 2280-bp genomic fragment from the *lip-1* promoter/enhancer region upstream of a minimal promoter (Fig. 2A). This transcriptional reporter displayed the up-regulation of LIP-1::GFP in P5.p and P7.p in all cases examined (Fig. 2C) ( $n = 30$ ), confirming that the induction of LIP-1 in 2°

VPCs is regulated at the transcriptional level. At later stages, LIP-1::GFP expression remained high in the descendants of P5.p and P7.p and low in the descendants of P6.p (Fig. 2, D and E). In the descendants of the uninduced VPCs (P3.p, P4.p, and P8.p), LIP-1::GFP expression increased after the cells had fused to the hypodermal syncytium *hyp7* where LIP-1::GFP was strongly expressed (Fig. 2E).

To investigate if LIP-1 was up-regulated in ectopic 2° cells, we examined LIP-1::GFP expression in *lin-15(rf)* (13) and *let-60(gf)* mutants in which all VPCs frequently adopt primary (1°) or 2° vulval fates. In 72% of *lin-15(rf)* ( $n = 18$ ) and 68% of *let-60(gf)* animals ( $n = 34$ ), LIP-1::GFP was up-regulated in P3.p, P4.p, or P8.p in addition to P5.p and P7.p (Fig. 2F). Moreover, in *lin-12 notch(gf)* mutants in which all VPCs adopt the 2° fate (14), up-regulation of LIP-1::GFP always occurred in all VPCs (Fig. 2G) ( $n = 20$ ). On the other hand, in *lin-12 notch(lf)* mutants, the induction of LIP-1::GFP in P5.p or P7.p was not observed, and LIP-1::GFP was expressed at low levels in all VPCs (Fig. 2H) ( $n = 23$ ) [note that the strong LIP-1::GFP expression in the *hyp7* nuclei P2.p and P9.p was unchanged in *lin-12(lf)* mutants]. Downstream of LIN-12, the lateral signal is transduced by a CSL (CBF-1/Suppressor of Hairless/LAG-1) transcription factor that binds to RTGGGAA motifs in the regulatory regions of the target genes (15). Likewise, the *lip-1* promoter/enhancer region contains a cluster of four potential CSL binding sites (Fig. 2A). Animals carrying a LIP-1::GFP reporter in which all four RTGGGAA motifs had been mutated to RAGGGAA did not show induction of LIP-1::GFP in P5.p or P7.p (Fig. 2I) ( $n = 26$ ), similar to the pattern observed in *lin-12(lf)* mutants. Thus, *lip-1* may be a direct target of the Notch signaling pathway in the VPCs.

LIN-12/NOTCH performs two functions during vulval induction that are separated by the phase of the VPC cell cycle (16). Before completion of the S phase, LIN-12 inhibits the specification of the 1° fate and maintains the VPCs in an uncommitted state. After completion of the S phase, LIN-12 promotes the specification of the 2° fate. To determine in which phase of the cell cycle the up-regulation of LIP-1 takes place, we arrested the VPCs in the S phase by transferring mid-L2 larvae to hydroxyurea-containing medium. In all hydroxyurea-arrested animals carrying the transcriptional reporter, LIP-1::GFP expression was up-regulated in P5.p and P7.p ( $n = 30$ ). Therefore, *lip-1* may be induced before the end of the S phase to prevent P5.p and P7.p from adopting the 1° fate (17).

To test this hypothesis, we asked if loss of *lip-1(+)* function allows neighboring VPCs to adopt the 1° fate. For this purpose, we compared the expression pattern of the 1° fate marker EGL-17::GFP (18) in the presence and absence of *lip-1(+)* activity. In *lip-1(lf)* single mutants, EGL-17::GFP was expressed exclusively in P6.p (Table 2, rows 1 and 2). However, when the activity of the RTK/RAS/MAPK signaling pathway

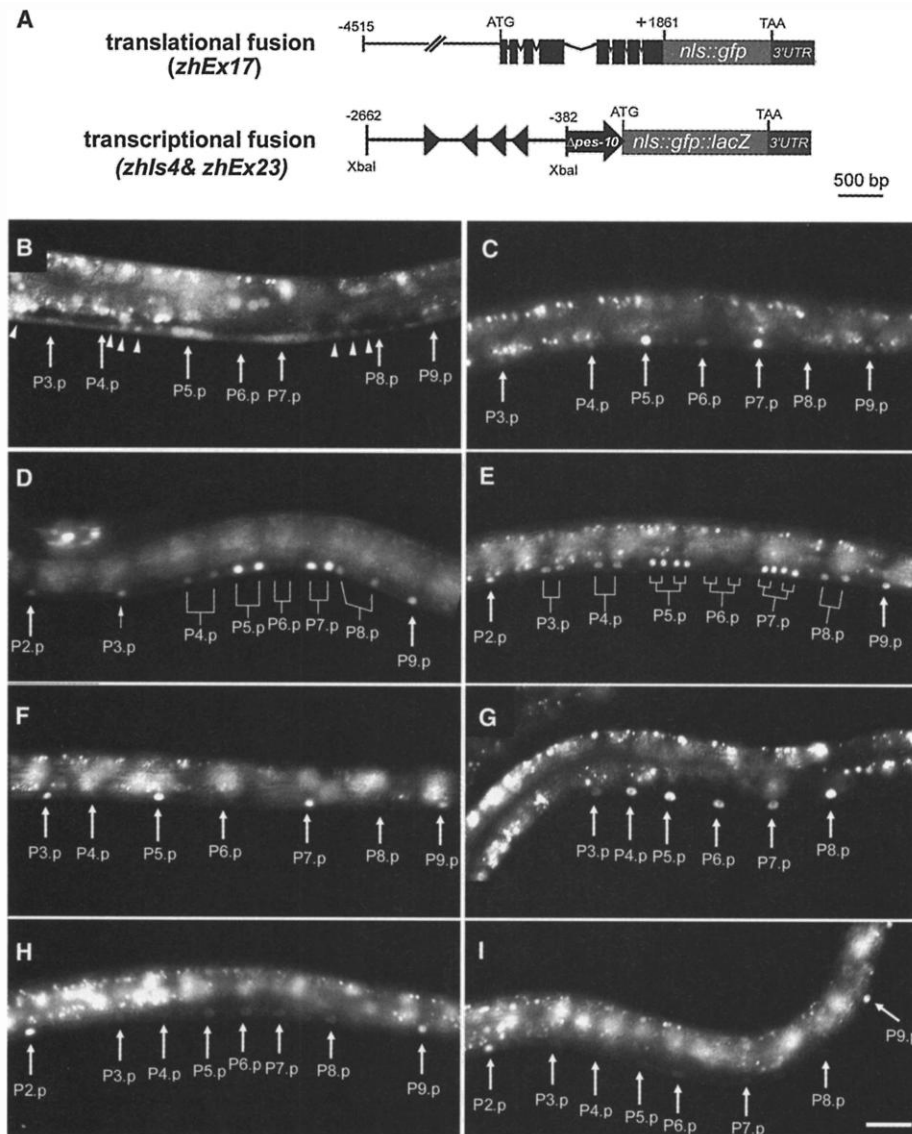


**Fig. 2.** (A) Structure of the rescuing translational LIP-1::GFP fusion *zhEx17[lip-1::nls::gfp]* (27) and the transcriptional fusion (*zhls4 & zhEx23*). The black triangles shown in the transcriptional fusion represent the four CSL binding motifs at positions  $-1439$ ,  $-1214$ ,  $-1094$ , and  $-913$ . The minimal  $\Delta pes-10$  promoter controlling *nls::gfp* was fused to *lacZ* to achieve entirely nuclear GFP localization. (B) LIP-1::GFP expression (translational fusion) in the Pn.p cells of an early L3 larva. The position of the Pn.p cell nuclei is indicated by the arrows; the smaller arrowheads indicate ventral cord neurons that expressed LIP-1::GFP. The transcriptional fusion is shown in (C) through (I). (C) LIP-1::GFP expression in the Pn.p cells of an early L3 larva; (D) in the daughters of the VPCs; and (E) in the granddaughters of P5.p through P7.p and the daughters of P3.p, P4.p, and P8.p after they had fused with *hyp7*, and (F) in the Pn.p cells of *let-60(n1046<sup>gf</sup>)*, (G) *lin-12(n137<sup>gf</sup>)*, and (H) *lin-12(n137n720<sup>lf</sup>)* early L3 larvae. In (G) and (H), the extrachromosomal array *zhEx23* was used because *zhls4* had integrated near the *lin-12* locus. (I) Expression of LIP-1::GFP from a reporter (*zhEx25*) containing point mutations in the four CSL binding motifs. Bar (I), 20  $\mu$ m.

REPORTS

was increased, loss of *lip-1(+)* function frequently caused two or more adjacent VPCs to express the 1° fate marker EGL-17::GFP (Table 2, rows 3 to 8). In most cases, EGL-17::GFP expression could be observed in P5.p or P7.p in addition to P6.p, indicating that P6.p failed to inhibit the 1° fate in its neighbors when *lip-1(+)* was absent.

The data presented here suggest the following model. LIP-1 is initially expressed at a low level in all VPCs to repress basal MPK-1 activity. The anchor cell signal overcomes this constitutive inhibition in P6.p to induce the 1° fate. The lateral signal from P6.p up-regulates the transcription of *lip-1* in P5.p and P7.p to reduce MPK-1 activity and thereby mediate the lateral

inhibition of the 1° fate in these cells. Low MPK-1 activity in P5.p and P7.p, combined with the lateral LIN-12 signal, specifies the 2° fate (19, 20). Because loss of *lip-1(+)* function is not sufficient to disrupt lateral inhibition (Table 2, row 2), additional inhibitory mechanisms may exist. For example, the expression of the receptor for the inductive signal, LET-23 epidermal growth factor receptor (EGFR), increases in P6.p and decreases in P5.p and P7.p toward the end of the L2 stage. LET-23 EGFR in P6.p appears to sequester most of the inductive signal LIN-3 EGF (21), whereas the down-regulation of LET-23 EGFR in P5.p and P7.p may desensitize these cells toward the inductive signal.

Lateral inhibition of the RTK/RAS/

MAPK signaling pathway by Notch has been observed in various cell types in different organisms (22–25). The model presented here may help explain how adjacent cells can translate the small differences in the amount of an extrinsic signal they receive into a binary decision, resulting in a defined pattern of cell fates.

References and Notes

1. M. Camps, A. Nichols, S. Arkinstall, *FASEB J.* **14**, 6 (2000).
2. For details on the materials and methods used, see the supplementary information on Science Online at [www.sciencemag.org/cgi/content/full/291/5506/1055/DC1](http://www.sciencemag.org/cgi/content/full/291/5506/1055/DC1).
3. M. R. Lackner, K. Kornfeld, L. M. Miller, H. R. Horvitz, S. K. Kim, *Genes Dev.* **8**, 160 (1994).
4. Y. Wu, M. Han, *Genes Dev.* **8**, 147 (1994).
5. R. V. Aroian, G. M. Lesa, P. W. Sternberg, *EMBO J.* **13**, 360 (1994).
6. J. S. Simske, S. M. Kaech, S. A. Harp, S. K. Kim, *Cell* **85**, 195 (1996).
7. S. G. Clark, M. J. Stern, H. R. Horvitz, *Nature* **356**, 340 (1992).
8. M. R. Lackner, S. K. Kim, *Genetics* **150**, 103 (1998).
9. S. Tuck, I. Greenwald, *Genes Dev.* **9**, 341 (1995).
10. P. B. Tan, M. R. Lackner, S. K. Kim, *Cell* **93**, 569 (1998).
11. G. J. Beitel, S. G. Clark, H. R. Horvitz, *Nature* **348**, 503 (1990).
12. G. J. Beitel, S. Tuck, I. Greenwald, H. R. Horvitz, *Genes Dev.* **9**, 3149 (1995).
13. E. L. Ferguson, H. R. Horvitz, *Genetics* **123**, 109 (1989).
14. I. S. Greenwald, P. W. Sternberg, H. R. Horvitz, *Cell* **34**, 435 (1983).
15. S. Christensen, V. Kodoyianni, M. Bosenberg, L. Friedman, J. Kimble, *Development* **122**, 1373 (1996).
16. V. Ambros, *Development* **126**, 1947 (1999).
17. P. W. Sternberg, *Nature* **335**, 551 (1988).
18. R. D. Burdine, C. S. Branda, M. J. Stern, *Development* **125**, 1083 (1998).
19. W. S. Katz, R. J. Hill, T. R. Clandinin, P. W. Sternberg, *Cell* **82**, 297 (1995).
20. J. S. Simske, S. K. Kim, *Nature* **375**, 142 (1995).
21. A. Hajnal, C. W. Whitfield, S. K. Kim, *Genes Dev.* **11**, 2715 (1997).
22. S. Artavanis-Tsakonas, M. D. Rand, R. J. Lake, *Science* **284**, 770 (1999).
23. J. V. Price, E. D. Savenye, D. Lum, A. Breikreutz, *Genetics* **147**, 1139 (1997).
24. P. zur Lage, A. P. Jarman, *Development* **126**, 3149 (1999).
25. T. Ikeya, S. Hayashi, *Development* **126**, 4455 (1999).
26. D. R. Alessi *et al.*, *Methods Enzymol.* **255**, 279 (1995).
27. *gals36[HS-mpk-1(+); lip-1(lf); zhEx17* animals displayed an average induction of 3.0 ( $n = 30$ ); compare with Table 1, row 12. In one animal, P6.p and P7.p adopted the 1° fate.
28. We thank E. Brunner, A. Dutt, E. Hafen, and R. Klemenz for critical review of the manuscript; T. Höchli and T. Bächli for their help with microscopy; A. Fire for the GFP reporter plasmids and  $\Delta pes-10$  promoter; J. Wang and S. Kim for strains overexpressing *mpk-1*; and the *Caenorhabditis elegans* Genetics Center for providing some of the strains used. Supported by grants from the Sassella Foundation and the Swiss National Science Foundation (A.H.).

11 September 2000; accepted 9 January 2001  
 Published online 25 January 2001;  
 10.1126/science.1055642  
 Include this information when citing this paper.

Table 1. Genetic interactions between *lip-1* and genes controlling vulval induction.

Row	Genotype*	Average induction†	Number
1	Wild-type	3.0	Many
2	<i>lip-1(lf)</i>	3.0	28
3	<i>let-23(rf)</i>	1.1	49
4	<i>let-23(rf); lip-1(lf)</i>	2.4	47
5	<i>lin-7(lf)</i>	0.3	26
6	<i>lin-7(lf); lip-1(lf)</i>	2.5	43
7	<i>sem-5(rf)</i>	1.1	48
8	<i>lip-1(lf); sem-5(rf)</i>	2.9	40
9	<i>mpk-1(rf)‡</i>	1.0	44
10	<i>mpk-1(rf); lip-1(lf)‡</i>	2.8	56
11	<i>[HS-mpk-1(+)]</i>	3.0	40
12	<i>[HS-mpk-1(+)]; lip-1(lf)</i>	5.9	22
13	<i>lin-25(rf)‡</i>	1.5	32
14	<i>lip-1(lf); lin-25(rf)‡</i>	2.1	46
15	<i>[lin-31-lip-1]</i>	0.8	40
16	<i>[lip-1::gfp]</i>	2.8	56
17	<i>[lip-1::nls::gfp]</i>	0.9	37
18	<i>let-60(gf)</i>	4.3	45
19	<i>let-60(gf); [lip-1::nls::gfp]</i>	3.0	23
20	<i>[HS-mpk-1(+)]‡</i>	5.6	41
21	<i>[HS-mpk-1(+)]; [lip-1::nls::gfp]‡</i>	3.0	51
22	<i>lin-1(rf)</i>	5.9	33
23	<i>lin-1(rf); [lip-1::nls::gfp]</i>	5.8	38

\*Alleles used: *lip-1(zh15)* (this study); *let-23(sy1)*, *lin-7(e1413)*, *sem-5(n2019)*, *mpk-1(oz140)*, *gals36[HS-mpk-1(+)*, *EF1 $\alpha$ -D-mek(+)*, *unc-30(+)]* (rows 11 and 12), *lin-25(n545)*, *zhEx22[lin-31-lip-1]*, *zhEx16[lip-1::gfp]*, and *zhEx17[lip-1::nls::gfp]* (all this study); *let-60(n1046<sup>gf</sup>)*, *gals37[HS-mpk-1(+)*, *EF1 $\alpha$ -D-mek(+)*, *unc-30(+)]* (rows 20 and 21), and *lin-1(n304)*. †Average induction indicates the average number of VPCs adopting induced (1° or 2°) fates per animal. ‡The phenotype of these strains was scored at 25°C.

Table 2. Loss of *lip-1(+)* function allows neighboring VPCs to adopt the 1° fate.

Row	Genotype*	% EGL-17::GFP expression†						No.
		P3.p	P4.p	P5.p	P6.p	P7.p	P8.p	
1	Wild-type	0	0	0	100	0	0	>50
2	<i>lip-1(lf)</i>	0	0	0	100	0	0	41
3	<i>lin-15(rf)</i>	25	71	0	100	4	79	24
4	<i>lin-15(rf); lip-1(lf)</i>	60	60	40	100	30	87	30
5	<i>let-60(gf)</i>	0	6	0	100	0	3	33
6	<i>let-60(gf) lip-1(lf)</i>	9	45	53	100	45	62	53
7	<i>[HS-mpk-1(+)]</i>	0	0	0	100	0	0	40
8	<i>[HS-mpk-1(+)]; lip-1(lf)</i>	0	19	44	100	50	44	32

\*Alleles used: *lip-1(zh15)*, *lin-15(n309)*, *let-60(n1046<sup>gf</sup>)*, *gals36[HS-mpk-1(+)*, *EF1 $\alpha$ -D-mek(+)*, *unc-30(+)]*. In addition, these strains carried the *ayIs4[egl-17::gfp]* reporter transgene. †The frequency at which EGL-17::GFP expression was observed in each VPC is indicated as a percentage.